Journal of the Taiwan Institute of Chemical Engineers 63 (2016) 430–435

Contents lists available at ScienceDirect

Journal of the Taiwan Institute of Chemical Engineers

journal homepage: www.elsevier.com/locate/jtice

Highly visible-light absorbing black TiO_2 nanocrystals synthesized by sol–gel method and subsequent heat treatment in low partial pressure H_2

Ming-Chung Wu[a,b,*], I-Chun Chang[a], Kai-Chi Hsiao[a], Wei-Kang Huang[a]

[a] Department of Chemical and Materials Engineering, College of Engineering, Chang Gung University, Taoyuan 33302, Taiwan
[b] Center for Reliability Sciences & Technologies, Chang Gung University, Taoyuan 33302, Taiwan

ARTICLE INFO

Article history:
Received 14 December 2015
Revised 16 February 2016
Accepted 18 February 2016
Available online 1 April 2016

Keywords:
Nanostructures
Photocatalyst
TiO_2
Photodegradation

ABSTRACT

We present here a novel method for producing highly visible-light absorbing black TiO_2 nanocrystals by combining sol–gel synthesis and subsequent heat treatment in low partial pressure H_2. The synthesized black TiO_2 nanocrystals with trivalent titanium, oxygen vacancies and structural defects show a significantly lowered optical bandgap in reference to white TiO_2. Photodegradation of methyl orange under visible light irradiation indicates the synthesized black TiO_2 is superior to the commercial TiO_2-P25. The developed process is simple, cost-effective, safe and allows producing a series of visible spectrum active catalysts without the need for metal doping or decoration.

1. Introduction

Many novel photocatalysts have been found to be active in the treatment of wastewaters for the broad range of organic pollutants that are used by industries and in daily life [1]. TiO_2 is often cited as the best choice for energy materials due to many advantages, such as being thermally and chemically stable, inexpensive, easy to produce and to use, and humanly and environmentally friendly. However, TiO_2 still have a great disadvantage due to its wide band gap (anatase~3.2 eV; rutile~3.0 eV). TiO_2 only utilizes ultraviolet irradiation of the solar radiation [2,3]. However, ultraviolet light only accounts for five percent of the energy of the sunlight. So, how to take advantage of visible band to increase the absorption becomes an important issue. Many efforts of doping various metals or non-metal onto TiO_2 in bulk or on surface have been carried out to enhance absorbing ability over the visible spectrum [4–9]. These results showed clear enhancement of activities. However, the photocatalytic activity of metal-doped TiO_2 photocatalysts substantially depends on the character and the concentration of the dopant ions, besides the method of preparation and its thermal and reductive treatment [10–16]. Moreover, some doping elements are also very costly.

Since the discovery of black titanium dioxide in 2011, this novel nanomaterial attracted considerable interest due to its optical absorption in visible spectrum, which makes it a very promising candidate in solar driven applications, such as air purification, antimicrobial coatings, wastewater treatment, hydrogen generation, solar cells and many others [17–19]. The significant improvement of visible light and infrared absorption compared to the conventional white TiO_2 is due to nanoscale disordered layer at the surface, which is typically induced by high pressure hydrogen thermal treatment. Based on the results, many studies have aimed to modify titanium dioxide morphology such as nanowire and nanotubes array titanium dioxide with hydrogenation or to develop a strategy to create a disorder layer at the surface of titanium dioxide in order to further improve the photocatalytic activity[20,21]. Core–shell structures having the disordered layer as shell and crystalline titanium dioxide as core were demonstrated. The oxygen vacancy in the disordered structure adds localized states below the conduction band minimum of black titanium dioxide resulting in a significant narrowing of band gap from 3.2 eV to 1.85 eV [22,23].

"Black" TiO_2 is usually prepared under high pressure hydrogen condition for long calcination time using various forms of TiO_2 nanoparticles as starting materials. Since hydrogen gas is highly flammable, the preparation process with high pressure and high temperature can be dangerous for large scale production [24,25]. In this work, we demonstrate an alternative approach that uses diluted H_2 (15% in N_2) at 1 bar pressure. Here, we start with a sol–gel derived precursor, which is subsequently annealed in 15% H_2

* Corresponding author at: Department of Chemical and Materials Engineering, College of Engineering, Chang Gung University, Taoyuan 33302, Taiwan. Tel.: +886 3 2118800x3545; fax: +886 3 2118800x5324.
E-mail address: mingchungwu@mail.cgu.edu.tw (M.-C. Wu).

http://dx.doi.org/10.1016/j.jtice.2016.02.026
1876-1070/

(balanced with N_2). The influence of calcination temperature on the photoinduced decolorization of methyl orange is investigated to understand the role of trivalent titanium, oxygen vacancies and structural defects.

2. Experimental

Titanium oxide gel were prepared by sol–gel method using 7.20 ml titanium isopropoxide (Sigma-Aldrich, $Ti(OCH(CH_3)_2)_4$, 98+%) as the precursor and 21.50 ml n-propanol (Acros Organics, C_3H_7OH, reagent grade) as the solvent. Control the pH value by adding 1.00 ml hydrochloric acid (Acros Organics, 37%) to the solution. Then, 1.00 ml deionized water was added to the solution. To study the effect of the atmosphere during the calcination process, the gel was calcined under the flow of different atmospheres, *i.e.* air, nitrogen (99.999%), and hydrogen/nitrogen mixture (15% H_2–85% N_2). The flow rates of various atmospheres are the same of 25 mL/min. After gelation, titanium oxide gel was immediately calcined under the flow of various atmospheres at various temperatures of 400, 450, 500, 500 and 600 °C, for 2 h, and its heating rate is 5 °C/min.

For Raman scattering spectra of the synthesized TiO_2 samples, anatase TiO_2 (Acros, 98+%, anatase powder) and rutile TiO_2 (Alfa Aesar, 99.5%, rutile powder), they were positioned on a high-resolution piezoelectric stage of the scanning microscopy (WiTec, Alpha300S) and were excited by a 632.8 nm He–Ne laser (25 mW). The laser beam was focused with a 10× objective lens (Nikon plane objective, NA ≈ 0.9), and the diameter of the focused laser beam was about 10 μm. Transmission electron microscopy (TEM, JEOL, JEM-ARM200FTH, Japan) was used to observe the microstructures of various synthesized TiO_2 samples, and X-ray diffractometer (XRD, Bruker, D2 phaser with Xflash 430, Germany) was used to measure the crystal structure. In addition, UV–vis absorption spectra of various synthesized TiO_2 samples were measured by absorption spectrophotometer (Jasco Analytical Instruments, V-630, Japan) in the 300–900 nm wavelength range. X-ray photoelectron spectrometry (XPS, ULVAC-PHI Inc., Japan) was used to examine the carbon concentration of various TiO_2 samples by using Al K_α radiation with a photoelectron take-off angle of 45° in high vacuum ($\sim 10^{-7}$ Torr).

The synthesized TiO_2 nanocrystals were tested in the degradation of methyl orange, which is a commonly used model reaction in photocatalysis. In a typical experiment, 20.0 mg of catalyst was sonicated for 10 min in 150 mL of 1.0 mg/L methyl orange (Acros Organics, pure) aqueous solution. The temperature of the mixture was kept near room temperature. The suspension was irradiated with visible lamps under vigorous stirring at ambient conditions. For visible light source, six pieces of lamps (Goodly F8T5/D visible lamp, and the power was 8.0 W) were placed in a hexagonal arrangement around the reactor. The distance between each lamp and reactor is about 5.0 cm. Before the actual photodegradation experiments, the suspensions were left to relax for 10 min in order to minimize the error of the dye concentration measurements caused by initial surface adsorption. After centrifuging for 15 min at 5000 rpm, the absorption spectrum of the retained methyl orange and its derivatives in the supernatant was recorded by absorption spectrophotometer (Jasco Analytical Instruments, V-630, Japan) in the 300–900 nm wavelength range.

3. Results and discussion

The various synthesized TiO_2 nanocatalysts were analyzed by Raman spectroscopy to observe the phase transformation in different atmospheres, *i.e.* air (Air), nitrogen (N_2) and hydrogen/nitrogen (H_2/N_2) mixture. For Fig. 1(a), the synthesized TiO_2 nanocrystal calcined at various temperatures under the flow of air for 2 h were

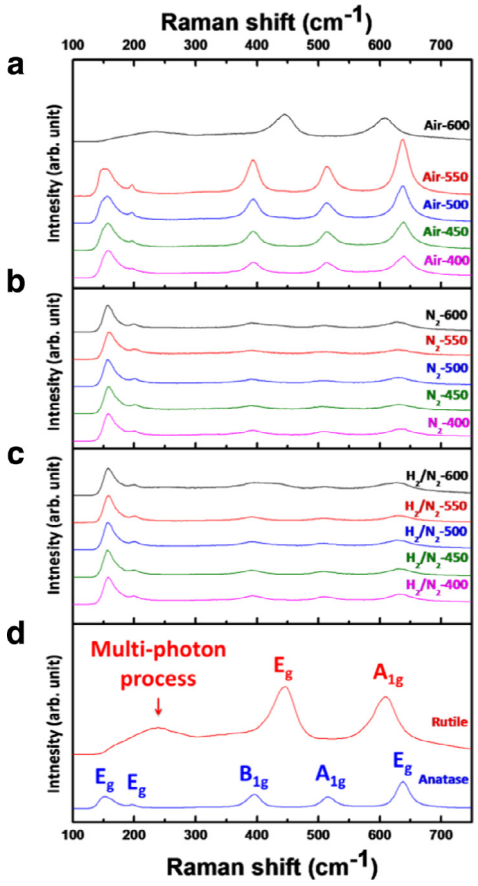

Fig. 1. Raman spectra of synthesized TiO_2 nanocrystals calcined at various temperatures of 400, 450, 500, 550 and 600 °C, for 2 h in different gaseous atmospheres of (a) air, (b) nitrogen, and (c) hydrogen/nitrogen mixture. (d) Raman spectra of the standard powders of anatase TiO_2 and rutile TiO_2.

denoted as TiO_2–Air–xxx, for which "xxx" indicates the calcination temperature. Raman spectra show that the synthesized TiO_2 nanocrystals calcined below 550 °C under the flow of air are having the anatase phase, which starts to transform to rutile once the calcination temperature reaches 600 °C. Raman spectra of titanium oxide precursor calcined in nitrogen and hydrogen/nitrogen mixture, are shown in Fig. 1(b) and (c), respectively. The results show the TiO_2 is a mixture of large amount of anatase and little amount of rutile phases. Hence, these atmospheres of N_2 or H_2/N_2 mixture could hinder the formation of rutile phase at 600 °C. In order to clearly understand the Raman spectra, anatase TiO_2 powder (Acros, 98+%) and rutile TiO_2 powder (Alfa Aesar, 99.5%) were used as a reference in this study. The anatase TiO_2 powder showed major Raman bands at 144, 200, 398, 515, 517 and 640 cm^{-1}, with the Raman bands at 515 cm^{-1} and 517 cm^{-1} superimposed, as shown in Fig. 1(d). These bands can be attributed to the six Raman-active modes of anatase phase with the symmetries of E_g, E_g, B_{1g}, A_{1g}, B_{1g}, and E_g, respectively [26]. For rutile TiO_2 powder, the typical Raman bands appear at 143, 243, 448 and 617 cm^{-1}, which can be ascribed to the B_{1g}, two-phonon scattering, E_g, and A_{1g} modes of rutile phase, respectively (Fig. 1(d)) [27]. E_g band that attributed to the O–Ti–O symmetric stretch vibration at TiO_2 bulk (144 cm^{-1}) and surface (640 cm^{-1}) increases dramatically when the calcination temperature is increased from 500 °C to 550 °C Fig. 1(a). However, the phenomena no longer existed in different gaseous atmosphere at the same calcined temperature, as show in Fig. 1(b) and (c). Because either in nitrogen or in hydrogen (H_2/N_2) atmosphere the oxygen vacancies and titanium trivalent ion had been induced

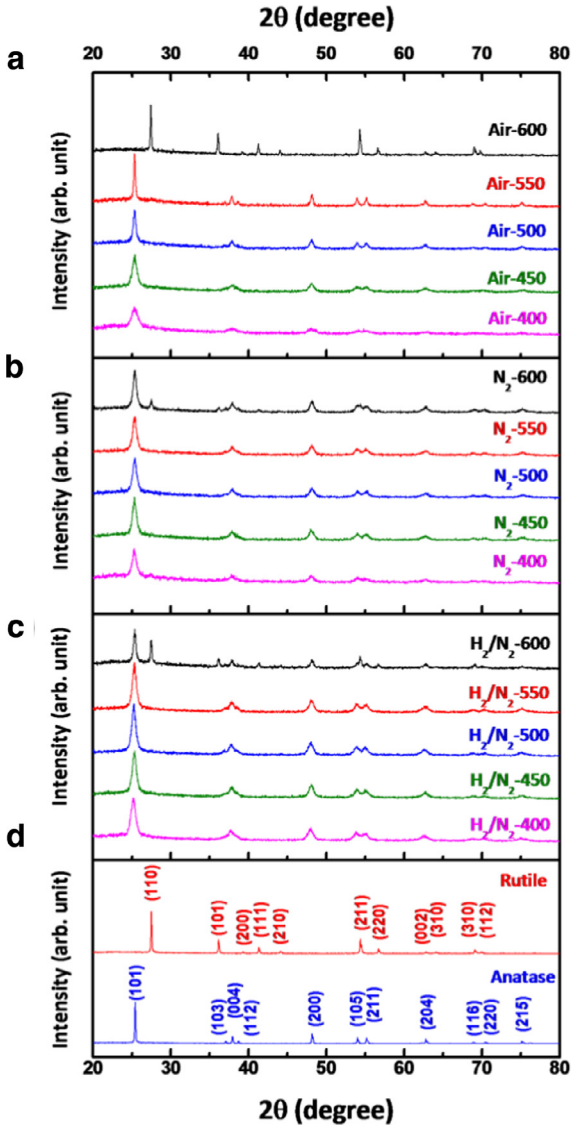

Fig. 2. X-ray diffraction patterns of synthesized TiO_2 nanocrystals calcined at various temperatures of 400, 450, 500, 550 and 600 °C, for 2 h in different gaseous atmospheres of (a) air, (b) nitrogen, and (c) hydrogen/nitrogen mixture. (d) X-ray diffraction patterns of the standard sample of anatase TiO_2 and rutile TiO_2.

during the calcination procedure, and therefore the signal of E_g band of TiO_2–N_2-550 and TiO_2–H_2/N_2-550 decreased significantly.

The crystal structure of various synthesized TiO_2 calcined under the flow of different atmospheres was also characterized by X-ray diffraction. XRD patterns of synthesized TiO_2 nanocrystals calcined at various temperatures under the flow of air (Fig. 2(a)), nitrogen (Fig. 2(b)), and hydrogen/nitrogen mixture (Fig. 2(c)), are shown in Fig. 2. The intensity of reflections at 2θ of 25.3° increased as calcination temperature increased to as high as 550 °C, because the increased calcination temperature improved the ordering of the anatase TiO_2 lattice. Moreover, the crystal structures exhibit the transformation from anatase to rutile phase from 550 °C to 600 °C for white TiO_2–Air series. For TiO_2–Air-600 as shown in Fig. 2(a), all XRD reflections can be perfectly indexed as the body-centered tetragonal unit cell of TiO_2 rutile, with unit cell parameters $a = b = 4.58$ Å, and $c = 2.96$ Å [Crystallography Open Database (COD) ID:4102355]. [28] For the synthesized TiO_2 nanocrystals calcined in N_2 or H_2/N_2 mixture below 550 °C as shown in Fig. 2(b) and (c), all diffraction peaks can be perfectly indexed as the body-centered tetragonal unit cell of TiO_2 anatase, with unit cell parameters $a = b = 3.78$ Å and $c = 9.52$ Å [COD ID:7206075]. [29] TiO_2–N_2-600 and TiO_2–H_2/N_2-600 showed the mixed TiO_2 phase consisting anatase and rutile, but TiO_2–Air-600 only exhibited rutile TiO_2 phase. The XRD results are consistent with those obtained by Raman measurements. The samples calcined in nitrogen or hydrogen/nitrogen mixture hindered the phase formation of TiO_2 rutile compared to the samples calcined in air. Hence, different atmospheric heat treatment resulted in the formation of different TiO_2 crystal structure.

Table 1
The concentration of oxygen and carbon in Air-400, Air-550, H_2/N_2-400 and H_2/N_2-550.

Samples	Chemical concentration (wt%)	
	Oxygen	Carbon
TiO_2–Air-400	12.16	3.08
TiO_2–Air-550	11.74	2.92
TiO_2–H_2/N_2-400	12.05	2.57
TiO_2–H_2/N_2-550	11.43	0.86

Camera images of synthesized TiO_2 nanocrystal powders obtained by calcination at temperatures between 300 °C and 600 °C (for 2 h) in various gaseous atmospheres are shown in Fig. 3. As the unique crystal structures were formed, the TiO_2 sample calcined in the nitrogen or hydrogen/nitrogen mixture were colorized black. The synthesized TiO_2 nanocrystals calcined at 300 °C or 350 °C could have the existence of carbon, so we only chose the synthesized TiO_2 nanocrystals calcined above 400 °C for further study.

The Kubelka–Munk function, *F(R)*, shows the optical absorbance of synthesized TiO_2 nanocrystals to be approximated from its reflectance. The Kubelka–Munk functions is given by

$$F(R) = (1-R)^2/2R = k/s = Ac/s$$

where R = reflectance; k = absorption coefficient; s = scattering coefficient; c = concentration of the absorbing species; A = absorbance. It gives a correlation between the reflectance and the concentrations of sample. From Fig. 4(a), the synthesized TiO_2-Air series only possessed UV band absorption, and did not cover the range in visible light. After the oxygen atom defects and/or trivalent titanium were formed in "black" TiO_2 catalysts (TiO_2–N_2 series or TiO_2–H_2/N_2 series), Kubelka–Munk function revealed a further enhancement compared with white TiO_2 (TiO_2–Air series) as shown in Fig. 4(b) and (c). For "black" TiO_2 catalysts (TiO_2–N_2 series and TiO_2–N_2/H_2 series), TiO_2–N_2-550 and TiO_2–H_2/N_2-550 showed the highest value of *F(R)*. However, the *F(R)* of "black" TiO_2 catalysts decreased when calcination temperature exceeded 550 °C. The reason could be due to the formation of TiO_2 rutile phase in black TiO_2 catalysts. From Fig. 4, we can observe that when titanium oxide precursor was calcined at various temperatures under the flow of N_2 or H_2/N_2 mixture, the absorbing spectrum clearly extends to the visible spectrum, which means that the band gap of the TiO_2 catalyst decreases as structural defects occurred in the TiO_2 lattice [24,25]. In order to confirm that the black color is not due to the existence of carbon, the chemical compositions of TiO_2–Air-400, TiO_2–Air-550, TiO_2–H_2/N_2-400 and TiO_2–H_2/N_2-550 were analyzed by X-ray photoelectron spectroscopy as shown in Table 1. Ti *2p* XPS spectra, O *1s* XPS spectra and C *1s* XPS spectra were show in Figs. S1–S3 of Supporting information, respectively. The oxygen concentration of TiO_2–H_2/N_2 series is always less than TiO_2–Air series at the same calcination temperature, because the insufficient oxygen surrounding could induce the oxygen vacancy when calcination procedure was carried out under H_2/N_2 atmosphere. Ti *2p* XPS spectra show the existence of Ti^{3+} signals at around 457.40 and 463.30 eV as shown in Fig. S1. The O *1s* spectra show the existence of O–H signal at around 531.00 eV as shown in Fig. S2. The XPS spectra show that induced oxygen vacancy in

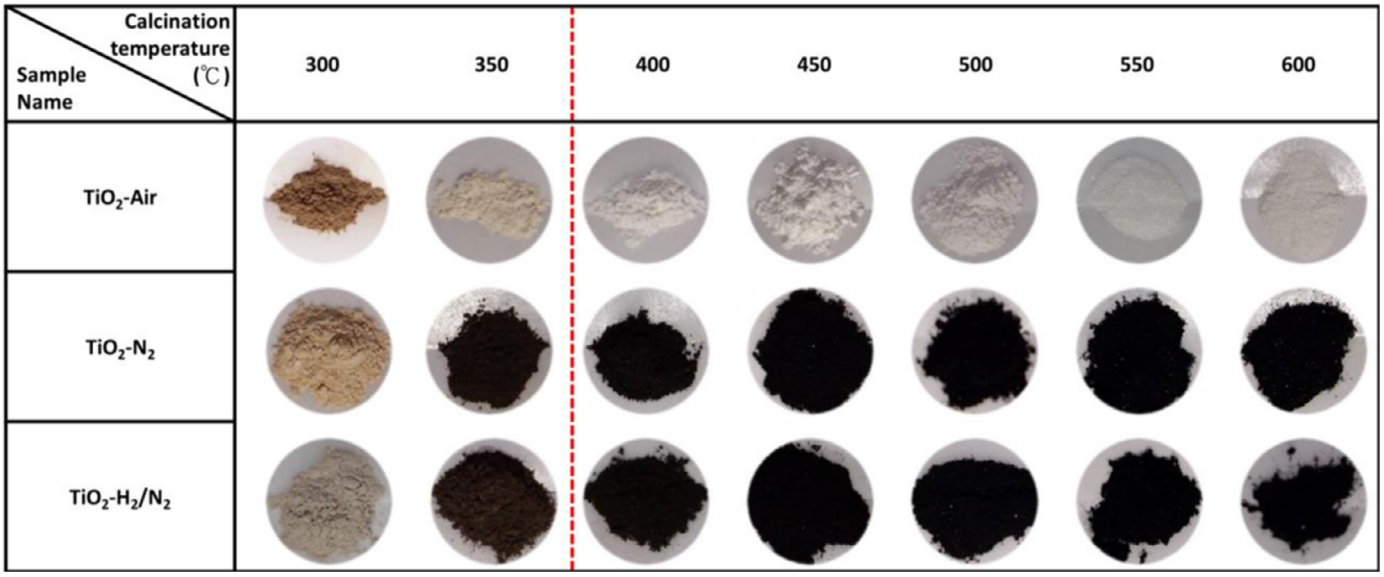

Fig. 3. Photo of synthesized TiO_2 nanocrystals calcined at various temperatures of 300, 350, 400, 450, 500, 550, and 600 °C, for 2 h in different gaseous atmospheres of air, nitrogen, and hydrogen/nitrogen mixture, respectively.

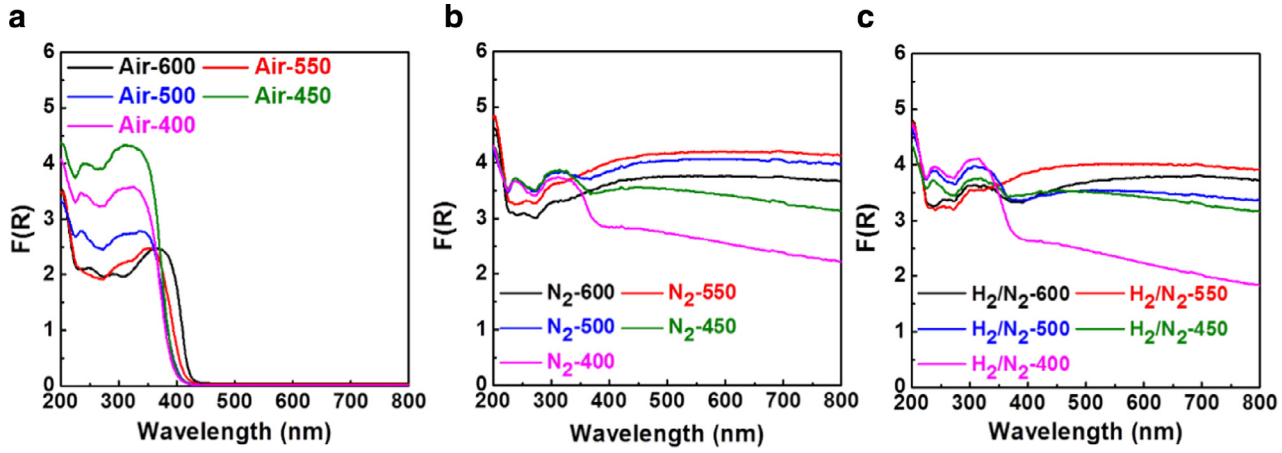

Fig. 4. Kubelka–Munk function of synthesized TiO_2 nanocrystals calcined at various temperatures of 400, 450, 500, 550, and 600 °C, for 2 h in different gaseous atmosphere of (a) air, (b) nitrogen and (c) hydrogen/nitrogen mixture, respectively.

TiO_2–H_2/N_2 series would interaction with hydrogen and form more O–H bonding compare with TiO_2–Air series. For carbon XPS spectra (Fig. S3), the carbon concentration of TiO_2–H_2/N_2–550 is 0.86 wt% much less than 2.92 wt% of TiO_2–Air-550, and the carbon concentration of TiO_2–H_2/N_2 series are always less than TiO_2–Air series at the same calcination temperature. The XPS results suggest that the color change is due to the presence of trivalent titanium and oxygen vacancies [21,22].

The microstructure of various synthesized TiO_2 calcined at 550 °C under different atmospheres were observed by HRTEM. The microstructure of TiO_2–Air-550, TiO_2–N_2-550 and TiO_2–H_2/N_2-550 were shown in Fig. 5(a)–(c), respectively. Fig. 5(□-1) showed TEM images of various synthesized TiO_2 nanocrystals, and their corresponding particle size distributions were shown in Fig. 5(□-2). The average particle sizes of TiO_2–Air-550, TiO_2–N_2-550 and TiO_2–H_2/N_2-550 are 19.5 nm, 10.1 nm and 10.2 nm, respectively. The results showed that the morphological scale of synthesized TiO_2 nanocrystals varied with the calcination atmosphere. The "black" TiO_2 (TiO_2–N_2-550 and TiO_2–H_2/N_2-550) has smaller particle size than that of white TiO_2 (TiO_2–Air-550) under the same thermal treatment. The average d_{101} spacing of various synthesized TiO_2 nanocrystals can be calculated from high-magnification lattice images as shown in Figs. Fig. 5(□-3). The direction of (101) crystal plane of each sample can be observed in the corresponding fast Fourier transformed pattern (Fig. 5(□-4)). Decreased d spacing of the (101) crystal plane is observed when comparing white TiO_2 to black TiO_2, and the change of (101) spacing is from 3.57 Å to 3.47 Å. The results suggest that calcination atmosphere results in the formation of trivalent titanium, oxygen vacancies and/or structural defects in the TiO_2 lattice. Furthermore, fine control of the morphology at nanoscales can still warrant additional research effort from a materials science point of view.

In order to obtain the optimal calcination process for each synthesized TiO_2 nanocrystals, titanium oxide precursor gel calcined in the flow of the various atmospheres at various temperatures of 400, 450, 500, 550, and 600 °C, were tested to find the highest photocatalytic activity under UV as well as visible light irradiation. For the photocatalytic activity of various synthesized TiO_2 nanocrystals, the absorption spectra of methyl orange as a function of UV irradiation time were recorded. Then, the absorbance measured at $\lambda = 464$ nm was used to calculate the methyl orange concentration using a calibration curve measured previously. The

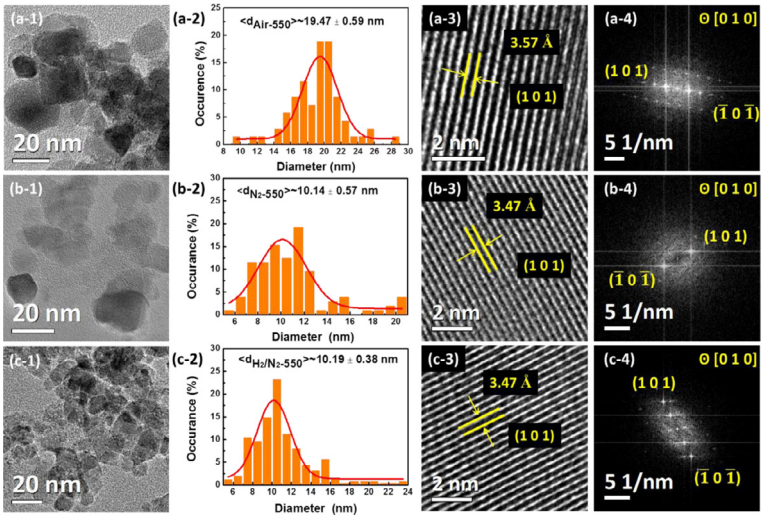

Fig. 5. TEM images of various synthesized TiO_2 nanocrystals calcined at 550 °C for 2 h in different gaseous atmosphere: (a) TiO_2–Air-550, (b) TiO_2–N_2-550, and (c) TiO_2–H_2/N_2-550. (□-1) the high-resolution TEM image, (□-2) the corresponding size distribution, (□-3) the high-magnification of the lattice, and (□-4) the corresponding fast Fourier transformed pattern of each sample.

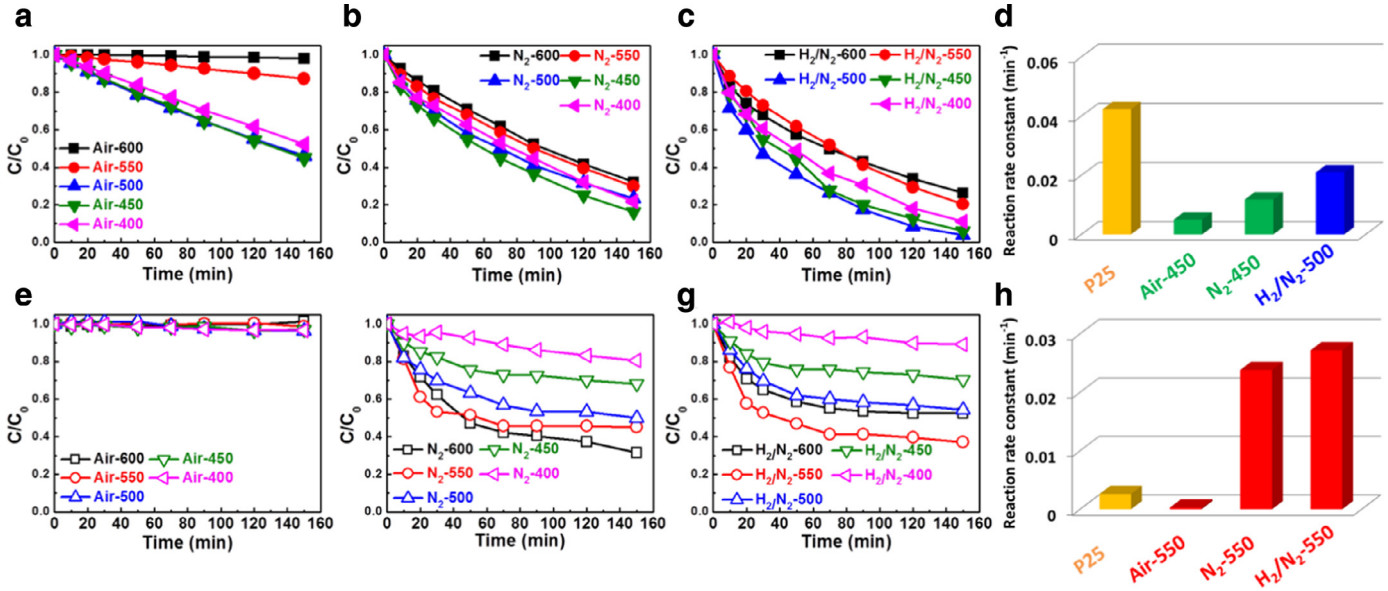

Fig. 6. The C/C_0 curve for the photodegradation of methyl orange at different time under (a–d) UV irradiation or (e–h) visible light irradiation using various synthesized TiO_2 nanocrystals calcined at various temperatures of 400, 450, 500, 550 and 600 °C, for 2 h in different gaseous atmosphere of (a, e) air, (b, f) nitrogen, and (c, g) hydrogen/nitrogen mixture. The reaction rate constants for the photodegradation of methyl orange of various synthesized TiO_2 nanocrystals under (d) UV irradiation or (h) visible light irradiation.

color of suspension changed from the initial orange color to colorless. The C/C_0 curve, where C is the concentration of the dye at time t and C_0 is the initial concentration, for the photodegradation of methyl orange at different time using various synthesized TiO_2 nanocrystals are shown in Fig. 6. For white TiO_2, TiO_2–Air-450 and TiO_2–Air-500 showed high photocatalytic activity under UV irradiation. However, TiO_2–Air-550 and TiO_2–Air-600 showed low photocatalytic activity due to the formation of large particles caused by high temperature calcination process.

For TiO_2–N_2 series, TiO_2–N_2-450 showed the highest photocatalytic activity under UV irradiation. For TiO_2–N_2/H_2 series, TiO_2–N_2/H_2-500 showed the highest photocatalytic activity under UV irradiation. In order to understand the correlation between the visible light degradation activities and calcination process for various TiO_2 catalysts, we also measured the photodegradation activities of various catalysts under visible light irradiations. For white TiO_2, all samples of TiO_2–Air series showed no visible light activity. The methyl orange decoloration rate *versus* various synthesized TiO_2 nanocrystals revealed that the calcination temperature of 550 °C produced the highest photodegradation activity of all "black" TiO_2 nanocrystals, including TiO_2–N_2 series and TiO_2–H_2/N_2 series.

From Fig. 4, much broader absorption was observed with increasing calcination temperature in the range of 400 °C–550 °C. However, TiO_2–H_2/N_2-600 showed lower photocatalytic activity compared to TiO_2–H_2/N_2-550 because of the lower absorption behavior in the visible band. From the results, there is a clear correlation between absorption behavior and photodegradation activity. TiO_2-catalyzed photodegradation of organic dyes usually follows Langmuir-Hinshelwood kinetics, which can be simplified to an apparent first-order kinetics at lower initial dye concentrations, mathematically described as $\ln(C_0/C) = kt$, and k is the apparent reaction rate constant [30,31]. Plotting the logarithm of the

reciprocal of the measured methyl orange concentration as a function of time, we obtained linear slopes for each catalyst we studied, in good agreement with the Langmuir–Hinshelwood model. The reaction rate constants for the degradation of methyl orange using various synthesized TiO_2 nanocrystals are shown using bar charts in Fig. 6(d) and (h). Under UV irradiation, TiO_2 P25 showed the highest photodegradation performance, and TiO_2–H_2/N_2-550 showed the second highest photodegradation performance. Actually, it is not easy to find a photocatalyst showing activity higher than that of TiO_2 P25, so it has been used as a standard TiO_2 photocatalyst 32–35. However, under visible light irradiation, TiO_2–H_2/N_2-550 showed the highest photodegradation activity under visible light irradiation due to its excellent photon absorption in the visible spectrum.

4. Conclusion

In this study, we developed black titanium dioxide nanoparticles using a Ti–O gel precursor (synthesized by sol–gel method) treated subsequently under different atmospheres, such as Air, N_2 (99.999%) and H_2/N_2 (15%/85%). The calcination process with the low partial pressure of hydrogen ensures safe production of black TiO_2 in contrast with the previously reported high pressure processes. The results indicate that our method can provide an easy pathway to achieve black TiO_2 by inducing oxygen vacancies at the surface of titanium dioxide. The obtained black TiO_2 shows excellent photocatalytic activity under visible irradiation without using lattice doping with metals or surface decoration with co-catalyst nanoparticles.

Acknowledgments

The authors appreciate Prof. Wei-Fang Su at National Taiwan University, Prof. Krisztián Kordás at Oulu University, and Dr. Ming-Tao Lee group (BL-13A1) at National Synchrotron Radiation Research Center for useful discussion and suggestions. The authors thank the staff at Instrumentation Center at National Tsing Hua University for the TEM microstructure analysis. The authors wish to acknowledge the financial support of the Ministry of Science and Technology, Taiwan (MOST 103-2221-E-182-008-MY2, MOST 104-2632-E-182-001, and MOST 105-3113-E-002-010) and the financial support of Chang Gung Memorial Hospital, Linkou, Taiwan (CMRPD2E0071).

Supplementary materials

Supplementary material associated with this article can be found, in the online version, at doi:10.1016/j.jtice.2016.02.026.

References

[1] Li Z, Cong S, Xu Y. Brookite vs anatase TiO_2 in the photocatalytic activity for organic degradation in water. ACS Catal 2014;4:3273–80.
[2] Zhu Z, Wu R-J. The degradation of formaldehyde using a Pt@TiO_2 nanoparticles in presence of visible light irradiation at room temperature. J Taiwan Inst Chem Eng 2015;50:276–81.
[3] Ni M, Leung MKH, Leung DYC, Sumathy K. A review and recent developments in photocatalytic water-splitting using TiO_2 for hydrogen production. Renew Sustain Energy Rev 2007;11:401–25.
[4] Anjana S, Andrey S, Anne-Riikka L, Krisztian K, Jyri-Pekka M, Pavel OP, Elena ST, Alexey PP, Maxim ED, Martina CM, Juergen L, Valery VT. Photocatalytic activity of TiO_2 nanoparticles: effect of thermal annealing under various gaseous atmospheres. Nanotechnology 2012;23:475711.
[5] Fox MA, Dulay MT. Heterogeneous photocatalysis. Chem Rev 1993;93:341–57.
[6] Marschall R, Wang L. Non-metal doping of transition metal oxides for visible–light photocatalysis. Catal Today 2014;225:111–35.
[7] Mu J, Chen B, Zhang M, Guo Z, Zhang P, Zhang Z, Sun Y, Shao C, Liu Y. Enhancement of the visible-light photocatalytic activity of In_2O_3–TiO_2 nanofiber heteroarchitectures. ACS Appl Mater Interfaces 2012;4:424–30.
[8] Wu M-C, Sápi A, Avila A, Szabó M, Hiltunen J, Huuhtanen M, Tóth G, Kukovecz Á, Kónya Z, Keiski R, Su W-F, Jantunen H, Kordás K. Enhanced photocatalytic activity of TiO_2 nanofibers and their flexible composite films: decomposition of organic dyes and efficient H2 generation from ethanol-water mixtures. Nano Res 2011;4:360–9.
[9] Zhang P, Yu Y, Wang E, Wang J, Yao J, Cao Y. Structure of nitrogen and zirconium Co-doped titania with enhanced visible-light photocatalytic activity. ACS Appl Mater Interfaces 2014;6:4622–9.
[10] Butburee T, Bai Y, Pan J, Zong X, Sun C, Liu G, Wang L. Step-wise controlled growth of metal@TiO_2 core–shells with plasmonic hot spots and their photocatalytic properties. J Mater Chem A 2014;2:12776–84.
[11] Ho W, Yu JC, Lee S. Synthesis of hierarchical nanoporous F-doped TiO_2 spheres with visible light photocatalytic activity. Chem Commun 2006;10:1115–17.
[12] Jiang X, Fu X, Zhang L, Meng S, Chen S. Photocatalytic reforming of glycerol for H_2 evolution on Pt/TiO_2: fundamental understanding the effect of co-catalyst Pt and the Pt deposition route. J Mater Chem A 2015;3:2271–82.
[13] Liu T, Zhang H. Novel Fe-doped anatase TiO_2 nanosheet hierarchical spheres with 94% {001} facets for efficient visible light photodegradation of organic dye. RSC Adv 2013;3:16255–8.
[14] Pandikumar A, Sivaranjani K, Gopinath CS, Ramaraj R. Aminosilicate sol–gel stabilized N-doped TiO_2–Au nanocomposite materials and their potential environmental remediation applications. RSC Adv 2013;3:13390–8.
[15] Pótári G, Madarász D, Nagy L, László B, Sápi A, Oszkó A, Kukovecz A, Erdőhelyi A, Kónya Z, Kiss J. Rh-induced support transformation phenomena in titanate nanowire and nanotube catalysts. Langmuir 2013;29:3061–72.
[16] Wang C, Chen Z, Jin H, Cao C, Li J, Mi Z. Enhancing visible-light photoelectrochemical water splitting through transition-metal doped TiO_2 nanorod arrays. J Mater Chem A 2014;2:17820–7.
[17] Chen X, Liu L, Yu PY, Mao SS. Increasing solar absorption for photocatalysis with black hydrogenated titanium dioxide nanocrystals. Science 2011;331:746–50.
[18] Xia T, Chen X. Revealing the structural properties of hydrogenated black TiO_2 nanocrystals. J Mater Chem A 2013;1:2983–9.
[19] Yu X, Kim B, Kim YK. Highly enhanced photoactivity of anatase TiO_2 nanocrystals by controlled hydrogenation-induced surface defects. ACS Catal 2013;3:2479–86.
[20] Juang R-S, Chen C-H. Comparative study on photocatalytic degradation of methomyl and parathion over UV-irradiated TiO_2 particles in aqueous solutions. J Taiwan Inst Chem Eng 2014;45:989–95.
[21] Cui H, Zhao W, Yang C, Yin H, Lin T, Shan Y, Xie Y, Gu H, Huang F. Black TiO_2 nanotube arrays for high-efficiency photoelectrochemical water-splitting. J Mater Chem A 2014;2:8612–16.
[22] Wang G, Wang H, Ling Y, Tang Y, Yang X, Fitzmorris RC, Wang C, Zhang JZ, Li Y. Hydrogen-treated TiO_2 nanowire arrays for photoelectrochemical water splitting. Nano Lett 2011;11:3026–33.
[23] Liu L, Yu PY, Chen X, Mao SS, Shen DZ. Hydrogenation and disorder in engineered black TiO_2. Phys Rev Lett 2013;111:065505.
[24] Naldoni A, Allieta M, Santangelo S, Marelli M, Fabbri F, Cappelli S, Bianchi CL, Psaro R, Dal Santo V. Effect of nature and location of defects on bandgap narrowing in black TiO_2 nanoparticles. J Am Chem Soc 2012;134:7600–3.
[25] Chen X, Liu L, Huang F. Black titanium dioxide (TiO_2) nanomaterials. Chem Soc Rev 2015;44:1861–85.
[26] Chen X, Liu L, Liu Z, Marcus MA, Wang W-C, Oyler NA, Grass ME, Mao B, Glans P-A, Yu PY, Guo J, Mao SS. Properties of disorder-engineered black titanium dioxide nanoparticles through hydrogenation. Sci Rep 2013;3:1510.
[27] Ohsaka T, Izumi F, Fujiki Y. Raman spectrum of anatase, TiO_2. J Raman Spectrosc 1978;7:321–4.
[28] Zhang J, Li M, Feng Z, Chen J, Li C. UV Raman spectroscopic study on TiO_2. I. Phase transformation at the surface and in the bulk. J Phys Chem B 2006;110:927–35.
[29] Dorolti E, Cario L, Corraze B, Janod E, Vaju C, Koo H-J, Kan E, Whangbo M-H. Half-metallic ferromagnetism and large negative magnetoresistance in the new lacunar spinel $GaTi_3VS_8$. J Am Chem Soc 2010;132:5704–10.
[30] Rezaee M, Mousavi Khoie SM, Liu KH. The role of brookite in mechanical activation of anatase-to-rutile transformation of nanocrystalline TiO_2: an XRD and Raman spectroscopy investigation. CrystEngComm 2011;13:5055–61.
[31] Katti A, Venna SR, Carreon MA. Self-assembly hydrothermal assisted synthesis of mesoporous anatase in the presence of ethylene glycol. Catal Commun 2009;10:2036–40.
[32] Wu M-C, Chih J-S, Huang W-K. Bismuth doping effect on TiO_2 nanofibres for morphological change and photocatalytic performance. CrystEngComm 2014;16:10692–9.
[33] Lu H, Zhao B, Pan R, Yao J, Qiu J, Luo L, Liu Y. Safe and facile hydrogenation of commercial Degussa P25 at room temperature with enhanced photocatalytic activity. RSC Adv 2014;4:1128–32.
[34] Wang X, Pehkonen SO, Ramo J, Vaananen M, Highfield JG, Laasonen K. Experimental and computational studies of nitrogen doped Degussa P25 TiO_2: application to visible-light driven photo-oxidation of As(III). Catal Sci Technol 2012;2:784–93.
[35] Wu M-C, Hiltunen J, Sápi A, Avila A, Larsson W, Liao H-C, Huuhtanen M, Tóth G, Shchukarev A, Laufer N, Á Kukovecz, Kónya Z, Mikkola J-P, Keiski R, Su W-F, Chen Y-F, Jantunen H, Ajayan PM, Vajtai R, Kordás K. Nitrogen-doped anatase nanofibers decorated with noble metal nanoparticles for photocatalytic production of hydrogen. ACS Nano 2011;5:5025–30.